

Protein Science

New insights into intracellular lipid binding proteins: The role of buried water

Christian Lücke, Sinian Huang, Martin Rademacher and Heinz Rüterjans

Protein Sci. 2002 11: 2382-2392

Access the most recent version at doi:[10.1110/ps.0212902](https://doi.org/10.1110/ps.0212902)

References

This article cites 38 articles, 14 of which can be accessed free at:
<http://www.proteinscience.org/cgi/content/full/11/10/2382#References>

Article cited in:
<http://www.proteinscience.org/cgi/content/full/11/10/2382#otherarticles>

Email alerting service

Receive free email alerts when new articles cite this article - sign up in the box at the top right corner of the article or [click here](#)

Notes

To subscribe to *Protein Science* go to:
<http://www.proteinscience.org/subscriptions/>

New insights into intracellular lipid binding proteins: The role of buried water

CHRISTIAN LÜCKE, SINIAN HUANG, MARTIN RADEMACHER, AND
HEINZ RÜTERJANS

Institut für Biophysikalische Chemie, Johann Wolfgang Goethe-Universität Frankfurt,
D-60439 Frankfurt am Main, Germany

(RECEIVED April 25, 2002; FINAL REVISION June 24, 2002; ACCEPTED June 28, 2002)

Abstract

The crystal structures of most intracellular lipid binding proteins (LBPs) show between 5 and 20 internally bound water molecules, depending on the presence or the absence of ligand inside the protein cavity. The structural and functional significance of these waters has been discussed for several LBPs based on studies that used various biophysical techniques. The present work focuses on two very different LBPs, heart-type fatty acid binding protein (H-FABP) and ileal lipid binding protein (ILBP). Using high-resolution nuclear magnetic resonance spectroscopy, certain resonances belonging to side-chain protons that are located inside the water-filled lipid binding cavity were observed. In the case of H-FABP, the pH- and temperature-dependent behavior of selected side-chain resonances (Ser82 O_H and the imidazole ring protons of His93) indicated an unusually slow exchange with the solvent, implying that the intricate hydrogen-bonding network of amino-acid side-chains and water molecules in the protein interior is very rigid. In addition, holo H-FABP appeared to display a reversible self-aggregation at physiological pH. For ILBP, on the other hand, a more solvent-accessible protein cavity was deduced based on the pH titration behavior of its histidine residues. Comparison with data from other LBPs implies that the evolutionary specialization of LBPs for certain ligand types was not only because of mutations of residues directly involved in ligand binding but also to a refinement of the internal water scaffold.

Keywords: Bound water; histidine titration; solvent exchange; protein backbone dynamics; lipid water interaction

In recent years, many studies were designed to elucidate the molecular details that define the binding characteristics of the various intracellular lipid binding proteins (LBPs). At present, this family of LBPs is divided into four evolutionary-derived categories (Hohoff and Spener 1998): (1) the cellular retinoid binding proteins; (2) ileal lipid binding protein (ILBP) and liver-type fatty acid binding protein (L-FABP); (3) intestinal-type FABP (I-FABP); and (4) adipocyte- (A-), brain- (B-), epidermal- (E-), heart- (H-), and myelin-type (M-) FABP. Even though all members of the

LBP family are characterized by a common three-dimensional fold (Banaszak et al. 1994), there are clear distinctions in their structural stabilities and ligand binding properties (Zimmerman et al. 2001) and in their protein backbone dynamics (Gutiérrez-González et al. 2002).

Both the structural and dynamic properties of the LBPs have been investigated extensively to date (Hanhoff et al. 2002). However, one important structural component inside the binding pocket has, for most part, been underrepresented in the general discussions about the structural integrity and binding properties of these proteins. Water molecules are always present inside the binding cavity of the LBPs, both in the ligand-free and complexed forms. Some of these water molecules have been observed as crystal water in the X-ray structures (Scapin et al. 1992; Cowan et al. 1993; Winter et al. 1993; Kleywegt et al. 1994; LaLonde et al.

Reprint requests to: Christian Lücke, Institut für Biophysikalische Chemie, Biozentrum, N230, 1. OG, Marie-Curie-Straße 9, 60439 Frankfurt a.M., Germany; e-mail: lueck@bpc.uni-frankfurt.de; fax: 49-69-79829632.

Article and publication are at <http://www.proteinscience.org/cgi/doi/10.1110/ps.0212902>.

1994; Young et al. 1994; Thompson et al. 1997; Hohoff et al. 1999; Balendiran et al. 2000; Folli et al. 2001). Others have been detected by nuclear magnetic resonance (NMR) spectroscopy, distinguishing between water molecules with different residence times (Mesgarzadeh et al. 1998; Wiesner et al. 1999; Likič et al. 2000). More recently, the possible influence of these internal water molecules on ligand binding has also been simulated by molecular dynamics calculations (Likič et al. 2000; Likič and Prendergast 2001; Bakowies and van Gunsteren 2002).

The presence of an intricate network of highly ordered water molecules has been thoroughly described for the X-ray structures of I-FABP, A-FABP, H-FABP, and cellular retinoic acid binding protein (CRABP)-II (Scapin et al. 1992; Kleywegt et al. 1994; LaLonde et al. 1994; Young et al. 1994). In the case of I-FABP and A-FABP, comparison of the apo and holo structures showed that certain crystal waters were displaced by the FA ligand on binding. But a significant number of ordered water molecules still remained at identical positions inside the protein cavity of the holo forms, located just next to the aliphatic hydrocarbon chain of the FA. It has been postulated that these crystal waters form a sort of hydration shell that interacts with the bound ligand. In holo I-FABP, these water molecules are located at the concave face of the slightly bent FA ligand (Sacchettini et al. 1992), whereas in the holo forms of A-FABP and H-FABP, the crystal waters are clustered beneath the pseudo-*re* face of the U-shaped FA (LaLonde et al. 1994; Young et al. 1994). In the latter two proteins, the binding cavity is divided into three sections, consisting of a cluster of hydrophobic side-chains at the bottom, a scaffold of polar and ionizable groups that interact with the bound water molecules in the middle part, and a mixture of residue types at the top where the FA rests near the entry portal. It has been proposed that simultaneous with the entry of the FA ligand into the binding cavity, the displaced water molecules exit through a second portal in the gap between β -strands D and E, thus driving the FA binding process (Sacchettini et al. 1992; Young et al. 1994). Moreover, an extensive hydrogen-bonding network of ionizable or polar side-chains and water molecules was shown to extend in H-FABP over a distance of 8.3 Å from Arg106 at the ligand binding site to Glu72 in the gap region, which in turn is connected to the external solvent (Young et al. 1994).

These crystallographic data subsequently raised the question of how fast the internally bound water molecules exchange with the external solvent when the protein is in solution. An NMR spectroscopic study on bovine H-FABP has reported that a total of 23 (apo form) and 21 (holo form) water molecules in direct contact with backbone amide protons showed residence times >300 ps (Mesgarzadeh et al. 1998). In the case of rat I-FABP, magnetic relaxation dispersion experiments indicated three (apo form) and four (holo form) long-lived water molecules with residence

times >10 ns, plus another 10 to 20 moderately ordered waters (Wiesner et al. 1999). Molecular dynamics simulations on fully solvated rat I-FABP have produced additional data on the water flux into and out of the binding cavity. One study reported ~20 internal water molecules with average residence times between 0.6 and 2.0 ns for the apo protein (Likič and Prendergast 2001), whereas a more recent publication specified 25 (apo form) and seven (holo form) internal waters with residence times >5 ns (Bakowies and van Gunsteren 2002).

Here we present results obtained for two very different LBPs, bovine H-FABP and porcine ILBP. Using multidimensional NMR techniques in solution, certain proton resonances have been tracked to study pH- and temperature-dependent effects that occur inside the protein cavity at different lipidation states. The resulting data shed new light on the exchange behavior of the internal water and the implications for ligand binding.

Results and Discussion

Bovine H-FABP

The solution structures of bovine and human H-FABP had been determined previously by high-resolution NMR spectroscopy (Lassen et al. 1995; Lücke et al. 2001). Their structural features are comparable to the crystal structure of human H-FABP (Young et al. 1994). The NMR structures do not show, however, that the spacious lipid binding cavity inside the protein contains highly ordered solvent molecules that rest above a hydrophobic cluster of aliphatic and aromatic side-chains (Fig. 1). The number of crystal waters is dependent on the presence or the absence of the FA ligand, which displaces several water molecules. Here we present NMR data that focuses on several selected side-chain protons located inside the H-FABP cavity. The results provide new insights about the exchange behavior of the internal water molecules and, subsequently, the overall architecture of the protein.

Slow-exchanging side-chain protons in H-FABP

The interior of holo H-FABP contains an intricate hydrogen-bonding network of amino-acid side-chains and 13 ordered water molecules that extends throughout the entire protein cavity (Fig. 2). This network spans 8.3 Å from the ligand binding site (Arg106, Arg126, and Tyr128) to Glu72 and continues onward to Asp76. The latter side-chain is accessible to the external solvent via a hydrogen bond with WAT158. However, the only direct contact of the internal water cluster with the bulk solvent is found near Glu72, where WAT182 shows a hydrogen-bond connectivity to the external WAT187.

dicates that at neutral pH, the exchange of these two protons with the solvent is in the millisecond range, with faster exchange rates at lower pH or higher temperatures. Hence, the residence times of the respective internal water molecules should be within a similar time scale, indicating that the intricate hydrogen-bonding network inside the binding cavity anchors the bound waters even more firmly than proposed for other LBPs.

In addition, a number of human H-FABP mutants have been investigated by NMR spectroscopy at pH 7.0 and 298 K (Zimmerman et al. 1999). All mutant protein spectra displayed the Ser82 O γ H and His93 N ϵ 2H resonances, except for the E72S and F64S mutants. In the case of the E72S protein, these missing resonance signals have to be attributed to the absence of the direct hydrogen-bond interactions to Glu72 (see Fig. 2). For the F64S mutant, however, the only plausible explanation is a significant disruption of the hydrogen-bonding network owing to the replacement of the Phe64 ring. Because FA binding is reduced 10% by the replacement of Phe64 (Zimmerman et al. 1999), these results support the hypothesis that the ordered water molecules inside the H-FABP binding pocket actually serve as a sort of hydration shell for the cluster of hydrophobic side-chains at the bottom of the cavity (see Fig. 1) and simultaneously play a role in the ligand binding process.

Histidine titration in H-FABP

Another approach to study the exchange of water between the protein cavity and the external solvent was to observe the pH titration behavior of the internal histidine residue in H-FABP by collecting two-dimensional NMR spectra at different pH values. As shown in Figure 3 (left panel), bovine H-FABP contains two histidine residues, His93 and His119, but only the former is located inside the binding cavity. Because the NMR signal of the external His119 imidazole ring is not always visible (possibly because of conformational exchange), its pH-dependent behavior was not determined.

A series of TOCSY spectra were collected with both apo and holo H-FABP at pH values between 4 and 9, tracking the titration behavior of the histidine H δ 2-H ϵ 1 cross-peaks. In the holo form (Fig. 4, bottom panels), the H δ 2-H ϵ 1 signal of His93 shows no change throughout the entire pH range, indicating that the imidazole ring does not titrate in the presence of the ligand. Furthermore, the weak signal intensity and relatively broad line-width indicate a reduced internal mobility. Hence, it can be concluded that His93 is solvent-inaccessible and immobilized in the ligand-bound state. Remarkably, the titration results are the same in the apo form (Fig. 4, top panels), with identical chemical shift values of the His93 ring resonances as in holo H-FABP.

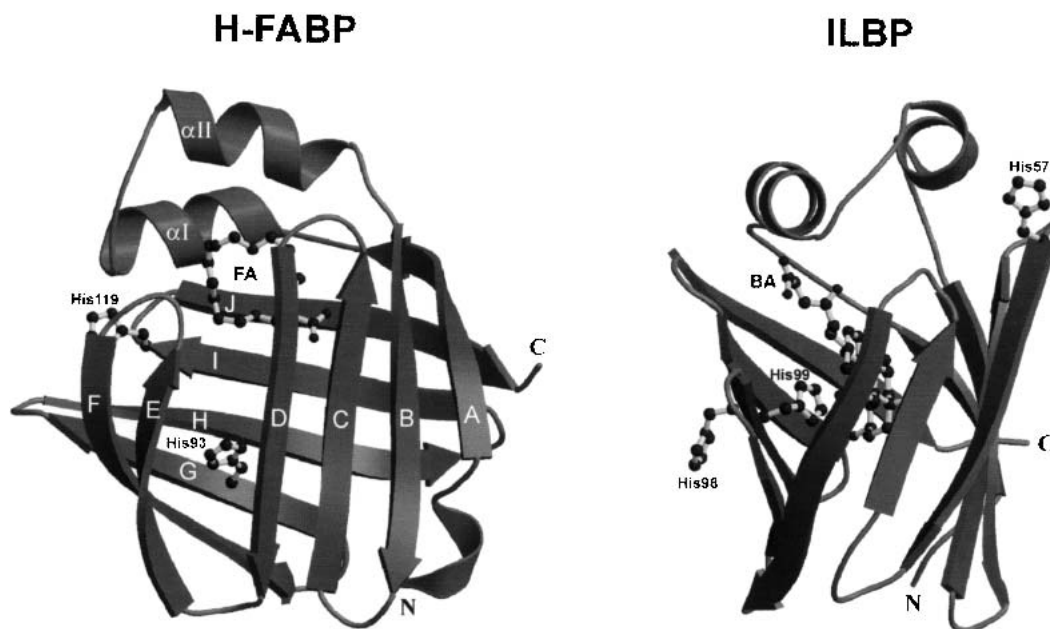


Fig. 3. Schematic ribbon diagrams of bovine H-FABP (*left*) and porcine ILBP (*right*). The histidine residues and ligand molecules (FA indicates fatty acid; BA, bile acid) are represented as ball-and-stick models. In H-FABP, the secondary structure elements consist of 10 antiparallel β -strands (A to J), two α -helices (I and II), and a helical loop at the N terminus. His93 is located inside the protein cavity, whereas the His119 side-chain is solvent-accessible on the protein surface. ILBP shows the same overall three-dimensional fold as H-FABP, except for the N-terminal helical loop. His99 is located in the binding site, whereas His57 and His98 are both solvent-accessible at the protein/solvent interface and on the protein surface, respectively. Produced with MOLSCRIPT (Kraulis 1991) and Raster3D (Merritt and Bacon 1997).

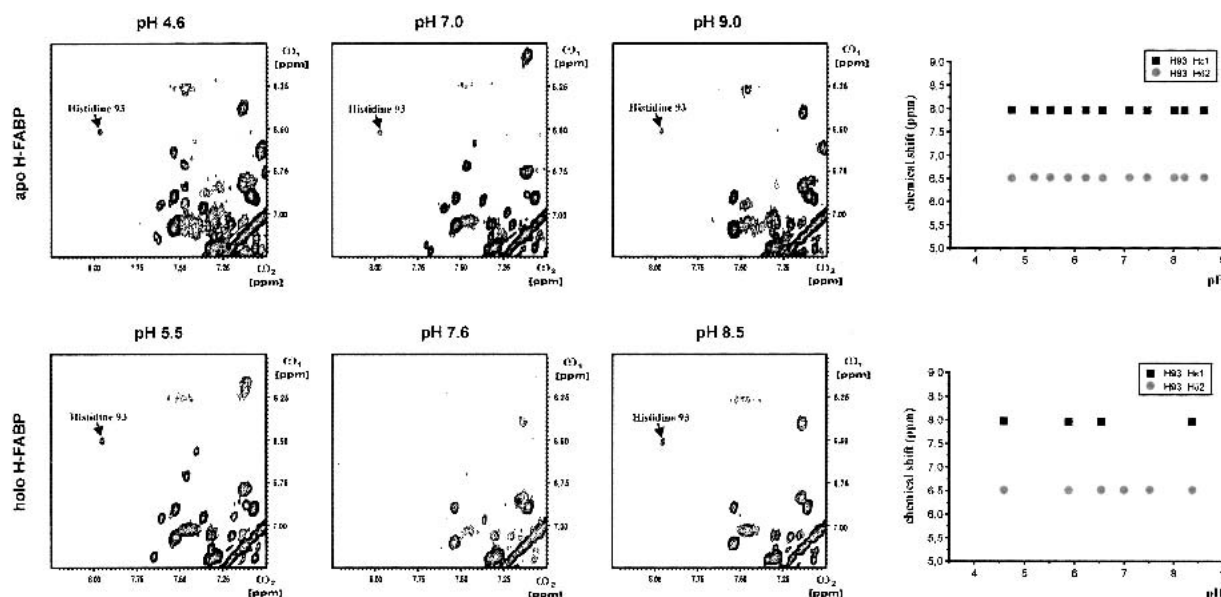


Fig. 4. Histidine titration in apo (*top*) and holo (*bottom*) H-FABP. The H δ 2-H ϵ 1 cross-peak of His93, with a weak and broad line shape that indicates a rather immobilized position of the imidazole ring system, have been labeled in the $^1\text{H}/^1\text{H}$ -TOCSY spectra at acidic, neutral, and basic pH values. The titration curves on the *right* show that the chemical shift values of H δ 2 and H ϵ 1 did not change on ligand binding or titration within the pH range 4 to 9, indicating a very similar, solvent-inaccessible arrangement of the H93 imidazole ring in both the ligand-free and the complexed protein. Enhanced line-broadening of the holo protein resonances at neutral pH, which caused the His93 signal to disappear, may be an indication of self-aggregation under physiological conditions.

Hence, we conclude that His93 remains solvent-inaccessible in the ligand-free form as well. Moreover, the micro-environment surrounding the His93 ring appears to be the same in both the apo and the holo protein, with a restricted mobility of the imidazole ring inside the protein cavity at all times. These results are in clear contrast to the histidine titration behavior of ILBP presented below.

Interestingly, at pH 7.0 and 7.6, the holo H-FABP samples showed an increased viscosity in combination with unusually large line-broadening in the NMR spectra, causing the His93 H δ 2-H ϵ 1 cross-peak to disappear completely. Consequently, the resonance assignments at these two pH values had to be derived from one-dimensional spectra, in which only the H δ 2 resonance could be unambiguously identified. The line shapes returned to normal width when the pH was shifted to acidic or basic values. This may be an indication of protein aggregation at neutral pH when the ligand is bound, whereas no such effect was observed in the apo form. A self-aggregation of H-FABP had been suggested previously by Fournier and Richard (1990), but the physiological significance of this effect remains to be elucidated.

To determine the protonation state of His93, long-range ^1H - ^{15}N -HSQC experiments were collected with bovine H-FABP (Fig. 5). Based on these spectra, the following resonance assignments were made for both apo and holo H-FABP at pH 5.8 and 298 K: His93 N δ 1, 251.3 ppm; H δ 2, 6.49 ppm; H ϵ 1, 7.90 ppm; N ϵ 2, 160.4 ppm; and H ϵ 2, 11.11

ppm. From these data, it can be concluded that the His93 imidazole ring is uncharged at pH 5.8, with the N ϵ 2 position protonated. Because His93 does not titrate in the pH range at which the protein is stable (pH 4 to 9), the His93 imidazole ring apparently remains neutral within the entire range both in the complexed and the ligand-free form. In addition, the tentative resonance assignments for His119 in the holo form (N δ 1, 199.7 ppm; H δ 2, 7.79 ppm; H ϵ 1, 8.26 ppm; and N ϵ 2, 175.1 ppm) indicate a charged state of the external, solvent-accessible His119 imidazole ring at pH 5.8 and 298 K.

Tyr19 ring flip in H-FABP

In summary, the data on H-FABP indicate a rather rigid, well-ordered microenvironment inside the binding pocket, which is not easily disturbed and apparently ensures a tight binding of the FA ligand in the lipid/protein complex. This overall conformational stability is also reflected by the fact that in holo H-FABP, the Tyr19 ring (see Fig. 1), which shows van der Waals contacts with the bound FA, displays separate resonance frequencies for the H δ 1/H δ 2 and H ϵ 1/H ϵ 2 proton pairs (Lücke et al. 1992, 2001), indicating an unusually slow ring flip when the FA is bound. This is the only such case in the LBP family reported to date. Separate Tyr19 ring resonances were also observed in nearly all H-FABP mutants (Zimmerman et al. 1999). Only in the apo form and in two Phe16 mutants (F16E and F16S), these ring proton resonances became degenerate. For apo H-FABP,

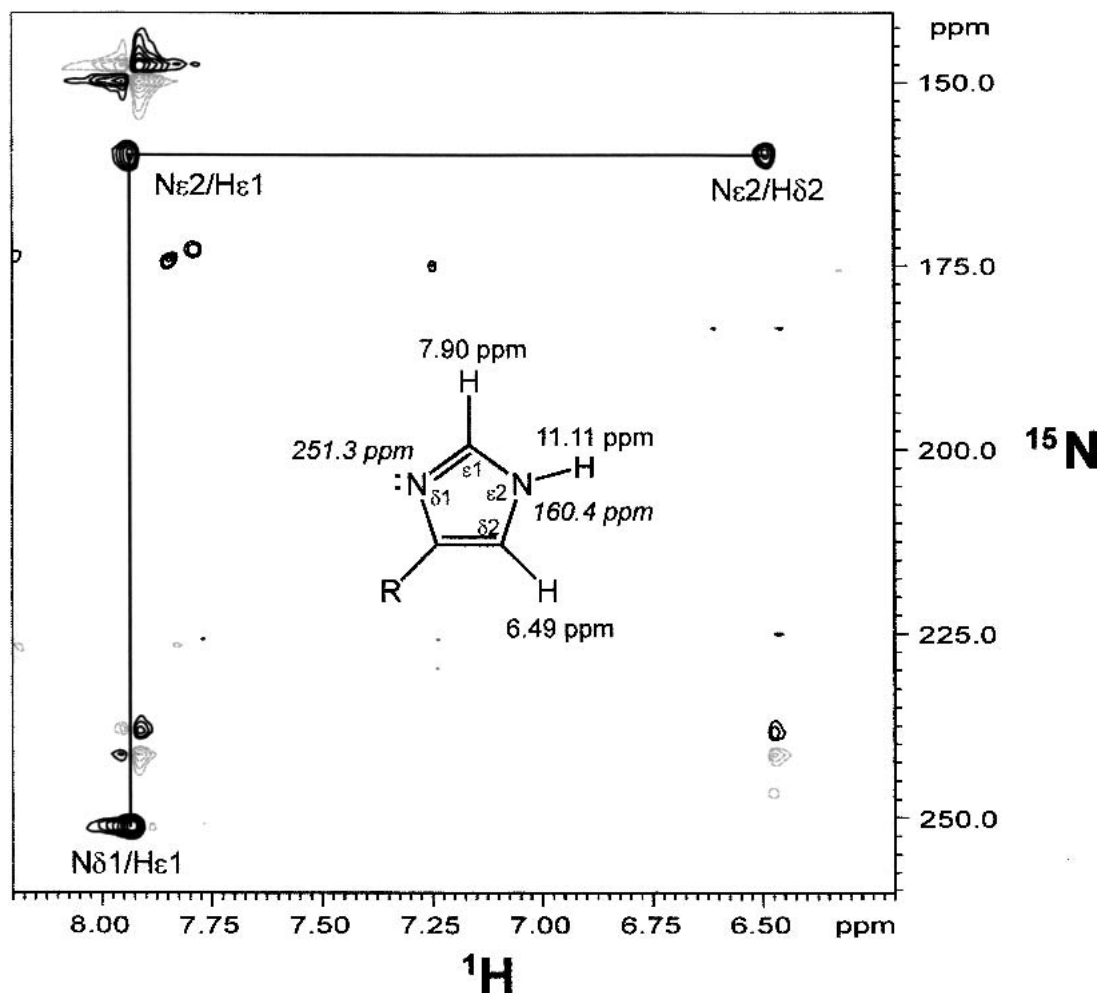


Fig. 5. Part of a long-range $^1\text{H}/^{15}\text{N}$ -HSQC spectrum of bovine holo H-FABP at pH 5.8 and 298 K. Peaks representing the $\text{N}\epsilon 2\text{-H}\delta 2$, $\text{N}\epsilon 2\text{-H}\epsilon 1$, and $\text{N}\delta 1\text{-H}\epsilon 1$ correlations of His93 are labeled. The chemical shift assignments of the imidazole resonances, as presented in the drawing of the chemical ring structure, indicate an uncharged state of His93 with the $\text{N}\epsilon 2$ position protonated. (Dashed spectral lines indicate negative intensities of dispersive signals that represent mirror artifacts of the actual His93 peaks.)

this can be explained by the missing ligand enabling the Tyr19 ring to rotate at a faster rate. In the case of the Phe16 mutants, apparently the replacement of the adjacent phenylalanine ring provides the Tyr19 phenol ring with more space for rotation.

Finally, the unusually rigid structure inside the H-FABP cavity compared with that of other LBPs is also reflected by the occurrence of up to four separate and stable conformational states in the portal region (Lücke et al. 2001), the unusually slow hydrogen/deuterium exchange behavior of the backbone amide protons in the β -strands (Lücke et al. 1992; Gutiérrez-González et al. 2002), and the limited number of exchange contributions in the backbone dynamics (Lücke et al. 1999).

Porcine ILBP

In contrast to H-FABP, the overall structure of ileal lipid binding protein (ILBP) appears to be more flexible, despite

the common three-dimensional fold (see Fig. 3). For ILBP, the hydrogen/deuterium exchange of backbone amide protons in the β -sheet occurs very fast (Lücke et al. 1996); the backbone dynamics behavior indicated an increased amount of exchange contributions on the millisecond-to-microsecond time scale (Lücke et al. 1999); no unusual occurrences like multiple backbone conformations or immobilized phenyl ring systems were observed; no slow-exchanging imidazole HN resonances were detected in the $^1\text{H}/^{15}\text{N}$ -HSQC spectra; and the protein stability is lower than for most other LBPs (Zimmerman et al. 2001).

Histidine titration in ILBP

Porcine ILBP contains three histidine residues (Fig. 3, right panel): one on the protein surface (His98), one at the protein/solvent interface (His57), and one in the ligand binding site (His99). The pH titration of ILBP in the apo form

showed changes of the imidazole proton resonances for all histidines (Fig. 6, upper panels), indicating that all three side-chains are freely solvent-accessible in the absence of ligand. Based on the changes in the chemical shifts, pK_a values of 6.18, 6.77, and 5.27 were determined for His57, His98, and His99, respectively. The rather low pK_a value for the internal His99 may be owing to electrostatic interactions with the nearby side-chain of Arg121 or to the hydrophobic environment created by other neighboring residues (Lücke et al. 2000).

In the holo protein, however, only His57 and His98 were titratable (Fig. 6, lower panels), with pK_a values of 6.71 and 6.53, respectively, whereas no titration behavior was observed for His99. The relatively weak signal intensity and broad line-width of the His99 resonances (below pH 5, only the diagonal signal of H δ 2 could be unambiguously assigned) indicate either a reduction in mobility or the occurrence of conformational exchange for this imidazole ring compared with His57 and His98. Hence, the bound bile acid ligand apparently interacts with the His99 side-chain and subsequently renders it inaccessible to the external solvent, as indicated by the solution structure of the glycocholate complex (Lücke et al. 2000). Moreover, although the external His98 shows no significant change of the pK_a value on ligand binding, the shift in the pK_a of His57 ($\Delta pK_a \sim 0.5$) seems to indicate that the presence of the bile acid ligand inside the protein cavity, or possibly of a second low-affinity ligand molecule at 298 K, as suggested recently by Tochrop and coworkers (2002), exerts a moderate influence on the local environment of His57.

In summary, the ILBP data imply a more penetrable binding cavity that shows faster exchange with the external solvent relative to that of H-FABP. Together with the fast hydrogen/deuterium exchange of the backbone amide protons in the β -sheet, these results provide additional support for a more flexible protein structure compared with other LBP family members.

Conclusions

From an evolutionary point of view, ILBP diverged much earlier from the common ancestral gene than did H-FABP, > 900 Myr ago, before the vertebrate/invertebrate split (Schaap et al. 2002). Hence, the ILBP structure may not have evolved to be as refined and specialized for its lipid binding tasks as other members of the LBP family. In fact, compared with other members of this protein family, the two 'earliest' LBPs, ILBP and L-FABP, both display an elevated amino-acid substitution rate, an array of different potential ligands, low lipid binding affinities, relatively low protein stabilities in the presence of urea, and fast hydrogen/deuterium exchange of the backbone amide protons (Muga et al. 1993; Lücke et al. 1996; Zimmerman et al. 2001; Schaap et al. 2002). ILBP is unique in the binding of bile

acid ligands, whereas L-FABP can incorporate two FA molecules at the same time. All other LBPs preferentially bind only a single ligand molecule with higher affinity, probably because of a specialization during evolutionary development. The internal cavity of H-FABP, on the other hand, apparently represents a very compact, highly specialized binding environment for long-chain FAs. This would explain the rather tight FA binding (Zimmerman et al. 2001), the relatively large number of long-lived internal water molecules (Mesgarzadeh et al. 1998), and the low backbone flexibility deduced from both hydrogen/deuterium exchange (Lücke et al. 1996; Gutiérrez-González et al. 2002) and backbone dynamics (Lücke et al. 1999), which have been observed for H-FABP relative to other LBP species.

Hence, it appears that the internal water structure of the LBPs plays a prominent role in defining their structural stability and their ligand binding properties. The variations in the amino-acid sequences, which have evolved over millions of years, optimized not only the direct protein/ligand interactions but also the arrangement of internal water as an integral part of the protein structure and an important factor in ligand binding. Most of the residues highlighted in Figure 2 are highly conserved in all members of LBP category 4 (Table 1), indicating a similar internal water structure as found in H-FABP. In the case of A-FABP, such a water network has already been shown by LaLonde et al. (1994). These well-ordered water molecules inside the protein cavity serve as a 'two-way hydrophobic hydration shell.' First, they shield the side-chains of the hydrophobic cluster at the bottom of the cavity from the solvent. Second, they provide the bound ligand with a hydration shell to compensate for part of the hydration energy the FA lost when entering the cavity. This setup makes the entire binding process energetically more favorable (Scapin et al. 1993) and also implies why the LBP structures usually become more stable on ligand binding (Lücke et al. 1996; Franzoni et al. 2002).

Another example of the great importance of water in these protein structures was given by a water molecule found in the gap region of the LBPs (Likič et al. 2000). This single solvent molecule, which is always associated with a very low B-factor value, interconnects β -turn DE and β -strand F via three hydrogen-bond interactions with protein backbone atoms, thus stabilizing the entire protein fold. In fact, this particular water molecule has also been recognized in the noncrystallographic LBP studies that focused on the solvent structure (Mesgarzadeh et al. 1998; Wiesner et al. 1999; Likič et al. 2000; Bakowies and van Gunsteren 2002).

The following question remains: How do the other LBPs fit into this internal water structure scheme? As mentioned before, the LBPs of category 4 present basically the same essential cavity residues as H-FABP, indicating a similar water arrangement. Most of these residues are also conserved in the CRABPs of category 1, in which a scaffold of

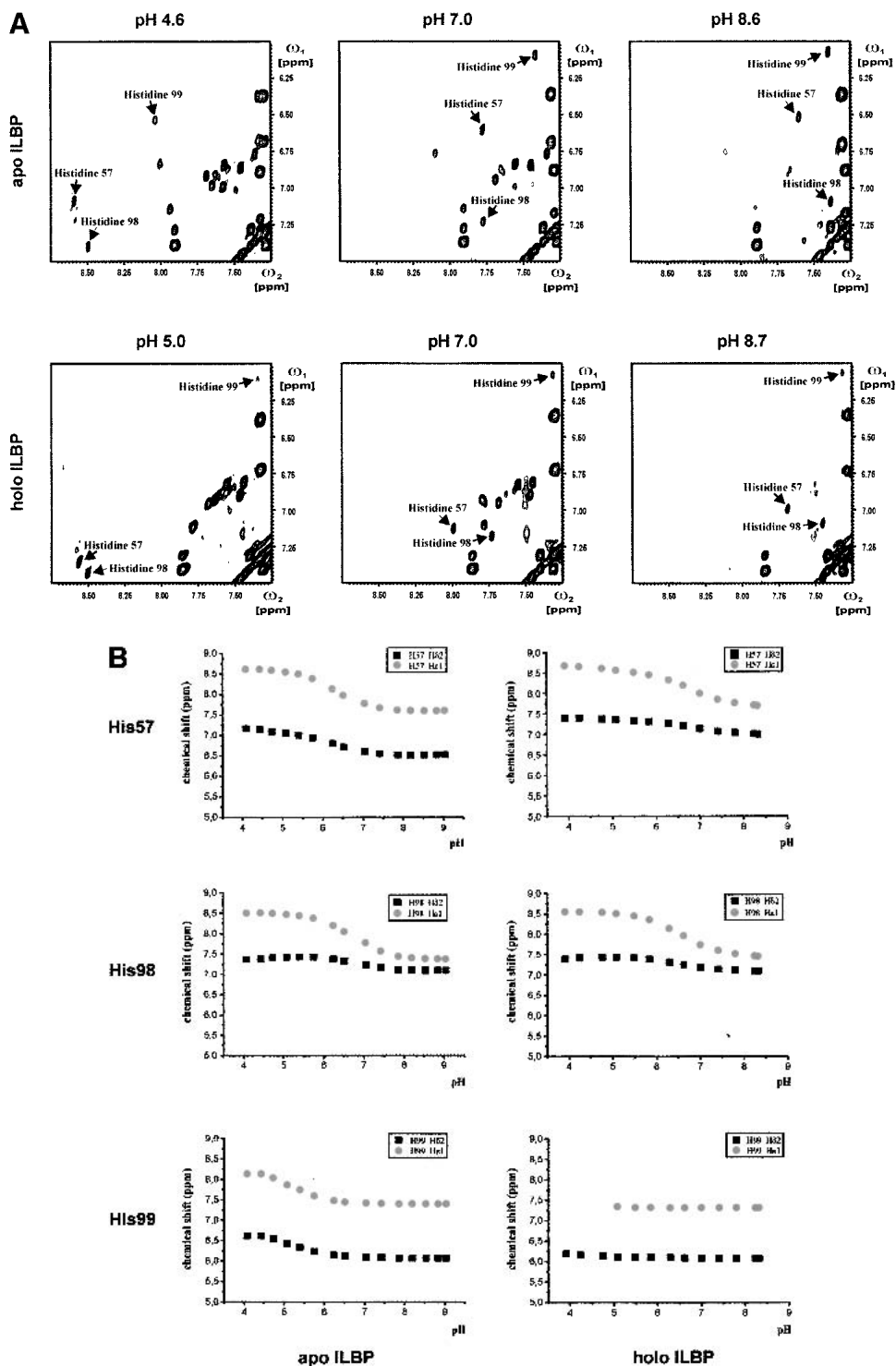


Fig. 6. Histidine titration in ILBP. (A) The H δ 2-H ϵ 1 cross-peaks of all three histidine residues have been labeled in the $^1\text{H}/^1\text{H}$ -TOCSY spectra of porcine apo (*top*) and holo (*bottom*) ILBP at acidic, neutral, and basic pH values. The His99 signal displays a broader and weaker line shape compared with that of the other two histidines. (B) Titration curves of all three histidine residues in porcine apo (*left*) and holo (*right*) ILBP. His57 (*top*) showed a pK_a change from 6.18 to 6.71 on ligand binding, indicating an influence of the ligand on the microenvironment of the His57 ring. The pK_a value of His98 (*middle*) did not change significantly between the apo and holo form, because this residue is located on the protein surface. The titration behavior of His99 (*bottom*), however, changed from a rather low pK_a value of 5.27 in the apo form to no titration effect within the pH range 4 to 9 in the holo form, indicating that the imidazole ring becomes solvent-inaccessible on ligand entry into the binding site.

Table 1. Sequence comparison of the residues shown in Fig. 2.

LBP	4	8	40	42	49	51	53	62	64	66	70	72	74	76	78	82	84	86	91	93	95	106	108	113	126	128
H-FABP	F	W	T	I	L	L	T	I	F	L	F	E	T	D	R	S	V	L	L	H	Q	R	L	L	R	Y
B-FABP	F	W	V	I	V	I	T	I	F	L	F	E	T	D	R	S	V	L	L	H	Q	R	I	M	R	Y
A-FABP	F	W	M	I	I	I	S	I	F	L	F	E	T	D	R	S	I	L	L	H	Q	R	R	L	R	Y
M-FABP	F	W	V	I	I	I	T	I	F	L	F	E	T	D	R	S	V	L	L	Q	Q	R	L	M	R	Y
E-FABP	L	W	C	I	L	I	T	F	C	L	F	E	T	D	R	T	C	F	L	Q	Q	R	L	L	R	Y
CRABP-I	F	W	V	I	F	I	T	I	F	V	F	E	T	D	R	S	A	W	I	C	Q	R	L	L	R	Y
CRABP-II	F	W	V	I	F	I	T	I	F	V	F	E	T	D	R	S	V	W	M	C	Q	R	L	L	R	Y
CRBP-I	F	W	K	I	M	I	T	M	F	V	F	E	L	D	R	T	V	W	L	C	Q	Q	I	L	Q	F
CRBP-II	Q	W	K	I	F	T	T	V	F	V	F	E	T	D	R	A	V	W	L	C	Q	Q	I	L	Q	F
CRBP-III	L	Y	K	I	M	V	T	V	F	V	F	E	L	D	R	T	V	W	L	C	Q	H	L	L	Q	F
I-FABP	F	W	L	I	F	V	E	V	F	L	F	Y	L	D	T	G	W	L	L	G	F	R	I	L	R	F
L-FABP	F	Y	S	I	F	F	I	N	F	V	C	L	T	T	E	T	V	L	L	T	F	T	L	I	R	S
ILBP	F	Y	S	V	F	W	Q	N	F	I	C	I	T	G	K	A	V	M	V	V	S	A	I	L	R	S

All lipid binding protein (LBP) sequences represent the human protein types, except for porcine ileal LBP. The numbering refers to the heart-type fatty acid binding protein (H-FABP) sequence. Residues that are identical in more than half of the sequences are highlighted in grey.

14 internal water molecules stretching from Arg111 to Gln97 and Glu73 (corresponding to Arg106, Gln95, and Glu72 in H-FABP, respectively) has been described for holo CRABP-II (Kleywegt et al. 1994). In the case of the cellular retinol binding proteins (CRBPs), the binding site residues (corresponding to Thr40, Arg106, Arg126, and Tyr128 in H-FABP) are different from the ‘acid-binding’ LBPs, but the other residues relevant for the internal water network are generally conserved. Moreover, a recent NMR study on CRBP-I (Franzoni et al. 2002) demonstrated that the positively charged Lys40, which interacts via a N-H... π hydrogen bond with the polyisoprene moiety of the retinol in the binding site, shows slow exchange of the N ζ amino protons, even in the apo protein, indicating a restricted solvent-accessibility of the protein cavity also in the absence of ligand.

The amino-acid sequences of LBPs in categories 2 and 3 are the most distinct from those of H-FABP. Hence, the cavity residues important for the creation of the internal water structure in H-FABP (see Fig. 2; Table 1) are generally not present at the corresponding sequence positions. Yet, in the case of I-FABP, the only member of LBP category 3, convergent evolution apparently produced a completely different arrangement of internal waters and bound FA compared with the FABPs in category 4. This internal water scaffold in I-FABP is not backed by a cluster of hydrophobic side-chains. Still, an intricate network of seven to eight water molecules serving as hydration shell for the bound FA, a slow exchange of backbone amide protons, a high protein stability, and strong FA binding (Sacchettini et al. 1992; Muga et al. 1993; Lücke et al. 1996; Zimmerman et al. 2001) all indicate an overall stable conformation analogous to the FABPs of LBP category 4.

Finally, for the two members of LBP category 2, ILBP and L-FABP, less stable structures were deduced from hydrogen/deuterium exchange of the backbone amides (Muga et al. 1993; Lücke et al. 1996) and from biochemical data

(Zimmerman et al. 2001). A greater solvent-accessibility of the binding cavity was also indicated by the second ligand entry portal of ILBP (Lücke et al. 2000). This additional entrance is caused by a deletion of residues in the β -turn GH (Sacchettini et al. 1990)—a feature that is found in the L-FABP sequence, too. Based on the results presented here for ILBP, we propose that the reason for the reduced binding affinities and specificities of the members of LBP category 2 is the lack of an extensive network of ordered water molecules inside the cavity to stabilize the overall structure. In fact, the only well-resolved X-ray structure known to date for a protein of this LBP category is that of rat L-FABP, with six crystal waters and one unknown heavy atom inside the binding cavity. None of the latter show hydrogen-bond interactions with each other, and only a single water and the unknown compound display van der Waals contacts with one of the FA ligands. This implies a lack of an intricate hydrogen-bonding network, in contrast to the other LBP categories. Hence, it may be concluded that the reduced structural stabilities and increased sequential variabilities of ILBP and L-FABP provide these two proteins with a greater versatility in function.

Of course, it will eventually be necessary to also distinguish between members of the same LBP category to further extend our knowledge on the different roles of water molecules in these lipid transporters. In LBP category 4, for example, the five different FABPs all bind long-chain FAs in the same U-shaped conformation as H-FABP. B-FABP, which is most closely related to H-FABP, shows very similar features in the NMR spectra: up to four separate spin-systems of residues in the portal region; slow exchange of Thr74 O γ 1H, Ser82 O γ H, and His93 N ϵ 2H; and unusually broad signals of the Tyr19 ring protons (Rademacher et al. 2002). This high degree of similarity between H-FABP and B-FABP is also reflected in their binding affinities and protein stabilities, whereas E-FABP, another member of LBP

category 4, behaves differently (Zimmerman et al. 2001). For E-FABP, which can bind a broader spectrum of long-chain FAs and eicosanoids (Hohoff et al. 1999; Schaap et al. 2002), a faster hydrogen/deuterium exchange of backbone amide protons and a larger number of exchange contributions on the millisecond-to-microsecond time scale indicated a higher backbone mobility compared with the solely FA-binding H-FABP (Gutiérrez-González et al. 2002). However, sequence differences between E-FABP and H-FABP that are related to ligand binding mostly involve mutations of the hydrophobic residues at the bottom of the binding cavity and a missing phenyl ring in the portal region (corresponding to Phe57 in H-FABP).

Clearly, not all details of this evolutionary development are fully understood at present. But the internal water as integral part of the LBP structures, with its obvious influence on the overall backbone dynamics, apparently plays a very significant role in the biological and physiological functions of these proteins.

Materials and methods

Bovine H-FABP and porcine ILBP have been prepared as previously described (Lassen et al. 1995; Lücke et al. 1996). Both proteins were delipidated using a Lipidex 5000 column (Glatz and Veerkamp 1983). H-FABP was relipidated with oleate (threefold excess), whereas ILBP was complexed with chenodeoxycholate (10-fold excess). The NMR samples generally consisted of 2 to 3 mM protein solutions in 20 mM phosphate buffer with 0.05% azide.

The NMR experiments were performed at either 298 or 310 K, using a Bruker DMX600 spectrometer operating at a ^1H resonance frequency of 600.13 MHz, and a 5-mm triple-resonance ($^1\text{H}/^{13}\text{C}/^{15}\text{N}$) probe with XYZ-gradient capability. One- and two-dimensional NMR experiments were recorded in a phase-sensitive mode with time-proportional phase incrementation of the initial pulse. Quadrature detection was applied in both dimensions with the carrier placed in the center of the spectrum on the water resonance. The water signal was suppressed by selective presaturation during the relaxation delay.

For the pH titration studies, $^1\text{H}/^1\text{H}$ -TOCSY spectra (80-ms spin-lock time) were acquired at 298 K within the pH range 4 to 9 (increments of ~ 0.4). Beyond these pH limits, the protein samples tended to precipitate. The cross-peaks resulting from scalar coupling between the H $\delta 2$ and H $\epsilon 1$ protons of the histidine imidazole rings were individually assigned. Analysis of the titration curves was performed using the Origin 2.90 software package (Micro-Cal).

The long-range $^1\text{H}/^{15}\text{N}$ -HSQC spectra were collected at both temperatures (298 and 310 K) and pH 5.8 (100 mM phosphate buffer). A 22-ms mixing period was used to refocus the single-bond correlations (Pelton et al. 1993). The spectral width in the ^{15}N dimension was set to 200.5 ppm, with the carrier placed at 150.9 ppm.

All spectra were calibrated with respect to 2,2-dimethyl-2-silapentane-5-sulfonate (Cambridge Isotope Laboratories) as an external reference (Wishart et al. 1995). The spectral data were processed on a Silicon Graphics workstation using the Bruker XWIN-NMR 1.3 software package. Baseline corrections of two-dimensional spectra were applied wherever necessary. Peak-pick-

ing and data analysis of the transformed spectra were performed with the AURELIA 2.5.9 program (Bruker). For structural analysis, the INSIGHT 97 software package (MSI) was used.

Acknowledgments

We thank Aukje W. Zimmerman, Herman T.B. van Moerkerk, and Jacques H. Veerkamp of the University of Nijmegen (The Netherlands) for providing the human H-FABP mutant proteins, as well as Ingrid Weber (University of Frankfurt) for assistance with the protein preparation work.

The publication costs of this article were defrayed in part by payment of page charges. This article must therefore be hereby marked "advertisement" in accordance with 18 USC section 1734 solely to indicate this fact.

References

- Bakowies, D. and van Gunsteren, W.F. 2002. Simulations of apo and holo-fatty acid binding protein: Structure and dynamics of protein, ligand and internal water. *J. Mol. Biol.* **315**: 713–736
- Balendiran, G.K., Schnütgen, F., Scapin, G., Borchers, T., Xhong, N., Lim, K., Godbout, R., Spener, F., and Sacchettini, J.C. 2000. Crystal structure and thermodynamic analysis of human brain fatty acid-binding protein. *J. Biol. Chem.* **275**: 27045–27054
- Banaszak, L., Winter, N., Xu, Z., Bernlohr, D., Cowan, S., and Jones, T.A. 1994. Lipid-binding proteins: A family of fatty acid and retinoid transport proteins. *Adv. Prot. Chem.* **45**: 89–151
- Cowan, S.W., Newcomer, M.E., and Jones, T.A. 1993. Crystallographic studies on a family of cellular lipophilic transport proteins: Refinement of P2 myelin protein and the structure determination and refinement of cellular retinol-binding protein in complex with all-*trans*-retinol. *J. Mol. Biol.* **230**: 1225–1246
- Folli, C., Calderone, V., Ottonello, S., Bolchi, A., Zanotti, G., Stoppini, M., and Rudolfo, B. 2001. Identification, retinoid binding, and X-ray analysis of a human retinol-binding protein. *Proc. Natl. Acad. Sci.* **98**: 3710–3715
- Fournier, N.C. and Richard, M.A. 1990. Role of fatty acid-binding protein in cardiac fatty acid oxidation. *Mol. Cell. Biochem.* **98**: 149–159
- Franzoni, L., Lücke, C., Pérez, C., Cavazzini, D., Rademacher, M., Ludwig, C., Spisni, A., Rossi, G.L., and Rüterjans, H. 2002. Structure and backbone dynamics of apo- and holo-cellular retinol-binding protein in solution. *J. Biol. Chem.* **277**: 21983–21997
- Glatz, J.F. and Veerkamp, J.H. 1983. A radiochemical procedure for the assay of fatty acid binding by proteins. *Anal. Biochem.* **132**: 89–95
- Gutiérrez-González, L.H., Ludwig, C., Hohoff, C., Rademacher, M., Hanhoff, T., Rüterjans, H., Spener, F., and Lücke, C. 2002. Solution structure and backbone dynamics of human epidermal-type fatty acid-binding protein (E-FABP). *Biochem. J.* **364**: 725–737
- Hanhoff, T., Lücke, C., and Spener, F. 2002. Insights into binding of fatty acids by fatty acid binding proteins. *Mol. Cell. Biochem.* (in press).
- Hohoff, C. and Spener, F. 1998. Fatty acid binding proteins and mammary-derived growth inhibitor. *Fett/Lipid* **100**: 252–263
- Hohoff, C., Borchers, T., Rüstow, B., Spener, F., and van Tilbeurgh, H. 1999. Expression, purification, and crystal structure determination of recombinant human epidermal-type fatty acid binding protein. *Biochemistry* **38**: 12229–12239
- Kleywegt, G.J., Bergfors, T., Senn, H., Le Motte, P., Gsell, B., Shudo, K., and Jones, T.A. 1994. Crystal structures of cellular retinoic acid binding proteins I and II in complex with all-*trans*-retinoic acid and a synthetic retinoid. *Structure* **2**: 1241–1258
- Kraulis, P.J. 1991. MOLSCRIPT: A program to produce both detailed and schematic plots of protein structures. *J. Appl. Crystallogr.* **24**: 946–950
- LaLonde, J.M., Bernlohr, D.A., and Banaszak, L.J. 1994. X-ray crystallographic structures of adipocyte lipid-binding protein complexed with palmitate and hexadecanesulfonic acid: Properties of cavity binding sites. *Biochemistry* **33**: 4885–4895
- Lassen, D., Lücke, C., Kveder, M., Mesgarzadeh, A., Schmidt, J.M., Specht, B., Lezius, A., Spener, F., and Rüterjans, H. 1995. Three-dimensional structure of bovine heart fatty-acid-binding protein with bound palmitic acid, determined by multidimensional NMR spectroscopy. *Eur. J. Biochem.* **230**: 266–280

- Likič, V.A. and Prendergast, F.G. 2001. Dynamics of internal water in fatty acid binding protein: Computer simulations and comparison with experiments. *Proteins* **43**: 65–72
- Likič, V.A., Juranič, N., Macura, S., and Prendergast, F.G. 2000. A “structural” water molecule in the family of fatty acid binding proteins. *Protein Sci.* **9**: 497–504
- Lücke, C., Lassen, D., Kreienkamp, H.-J., Spener, F., and Rüterjans, H. 1992. Sequence-specific ¹H-NMR assignment and determination of the secondary structure of bovine heart fatty acid-binding protein. *Eur. J. Biochem.* **210**: 901–910
- Lücke, C., Zhang, F., Rüterjans, H., Hamilton, J.A., and Sacchettini, J.C. 1996. Flexibility is a likely determinant of binding specificity in the case of ileal lipid binding protein. *Structure* **4**: 785–800
- Lücke, C., Fushman, D., Ludwig, C., Hamilton, J.A., Sacchettini, J.C., and Rüterjans, H. 1999. A comparative study of the backbone dynamics of two closely related lipid binding proteins: Bovine heart fatty acid binding protein and porcine ileal lipid binding protein. *Mol. Cell. Biochem.* **192**: 109–121
- Lücke, C., Zhang, F., Hamilton, J.A., Sacchettini, J.C., and Rüterjans, H. 2000. Solution structure of ileal lipid binding protein in complex with glycocholate. *Eur. J. Biochem.* **267**: 2929–2938
- Lücke, C., Rademacher, M., Zimmerman, A.W., van Moerkerk, H.T.B., Veerkamp, J.H., and Rüterjans, H. 2001. Spin-system heterogeneities indicate a selected-fit mechanism in fatty acid binding to heart-type fatty acid-binding protein (H-FABP). *Biochem. J.* **354**: 259–266
- Merritt, E.A. and Bacon, D.J. 1997. Raster3D: Photorealistic molecular graphics. *Methods Enzymol.* **277**: 505–524
- Mesgarzadeh, A., Pfeiffer, S., Engelke, J., Lassen, D., and Rüterjans, H. 1998. Bound water in apo and holo bovine heart fatty-acid-binding protein determined by heteronuclear NMR spectroscopy. *Eur. J. Biochem.* **251**: 781–786
- Muga, A., Cistola, D.P., and Mantsch, H.H. 1993. A comparative study of the conformational properties of *Escherichia coli*-derived rat intestinal and liver fatty acid binding proteins. *Biochim. Biophys. Acta* **1162**: 291–296
- Nicholls, A., Sharp, K.A., and Honig, B. 1991. Protein folding and association: Insights from the interfacial and thermodynamic properties of hydrocarbons. *Proteins* **11**: 281–296
- Pelton, J.G., Torchia, D.A., Meadow, N.D., and Roseman, S. 1993. Tautomeric states of the active-site histidines of phosphorylated and unphosphorylated III^{Glc}, a signal-transducing protein from *Escherichia coli*, using two-dimensional heteronuclear NMR techniques. *Protein Sci.* **2**: 543–558
- Rademacher, M., Zimmerman, A.W., Rüterjans, H., Veerkamp, J.H., and Lücke, C. 2002. Solution structure of fatty acid-binding protein from human brain. *Mol. Cell. Biochem.* (in press).
- Sacchettini, J.C., Hauff, S.M., Van Camp, S.L., Cistola, D.P., and Gordon, J.I. 1990. Developmental and structural studies of an intracellular lipid binding protein expressed in the ileal epithelium. *J. Biol. Chem.* **265**: 19199–19207
- Sacchettini, J.C., Scapin, G., Gopaul, D., and Gordon, J.I. 1992. Refinement of the structure of *Escherichia coli*-derived rat intestinal fatty acid binding protein with bound oleate to 1.75-Å resolution. *J. Biol. Chem.* **267**: 23534–23545
- Scapin, G., Gordon, J.I., and Sacchettini, J.C. 1992. Refinement of the structure of recombinant rat intestinal fatty acid-binding apoprotein at 1.2-Å resolution. *J. Biol. Chem.* **267**: 4253–4269
- Scapin, G., Young, A.C.M., Kromminga, A., Veerkamp, J.H., Gordon, J.I., and Sacchettini, J.C. 1993. High resolution X-ray studies of mammalian intestinal and muscle fatty acid-binding proteins provide an opportunity for defining the chemical nature of fatty acid:protein interactions. *Mol. Cell. Biochem.* **123**: 3–13
- Schaap, F.G., van der Vusse, G.J., and Glatz, J.F.C. 2002. Evolution of the family of intracellular lipid binding proteins in vertebrates. *Mol. Cell. Biochem.* (in press).
- Thompson, J., Winter, N., Terwey, D., Bratt, J., and Banaszak, L. 1997. The crystal structure of the liver fatty acid-binding protein. *J. Biol. Chem.* **272**: 7140–7150
- Tochtrop, G.P., Richter, K., Tang, C., Toner, J.J., Covey, D.F., and Cistola, D.P. 2002. Energetics by NMR: Site-specific binding in a positively cooperative system. *Proc. Natl. Acad. Sci.* **99**: 1847–1852
- Wiesner, S., Kurian, E., Prendergast, F.G., and Halle, B. 1999. Water molecules in the binding cavity of intestinal fatty acid binding protein: Dynamic characterization by water ¹⁷O and ²H magnetic relaxation dispersion. *J. Mol. Biol.* **286**: 233–246
- Winter, N.S., Bratt, J.M., and Banaszak, L.J. 1993. Crystal structures of holo and apo-cellular retinol-binding protein II. *J. Mol. Biol.* **230**: 1247–1259
- Wishart, D.S., Bigam, C.G., Yao, J., Abildgaard, F., Dyson, H.J., Oldfield, E., Markley, J.L., and Sykes, B.D. 1995. ¹H, ¹³C and ¹⁵N chemical shift referencing in biomolecular NMR. *J. Biomol. NMR* **6**: 135–140
- Young, A.C.M., Scapin, G., Kromminga, A., Patel, S.B., Veerkamp, J.H., and Sacchettini, J.C. 1994. Structural studies on human muscle fatty acid binding protein at 1.4 Å resolution: Binding interactions with three C18 fatty acids. *Structure* **2**: 523–534
- Zimmerman, A.W., Rademacher, M., Rüterjans, H., Lücke, C., and Veerkamp, J.H. 1999. Functional and conformational characterization of new mutants of heart fatty acid-binding protein. *Biochem. J.* **344**: 495–501
- Zimmerman, A.W., van Moerkerk, H.T.B., and Veerkamp, J.H. 2001. Ligand specificity and conformational stability of human fatty acid-binding proteins. *Int. J. Biochem. Cell Biol.* **33**: 865–876.